ACS APPLIED MATERIALS & INTERFACES

Research Article

www.acsami.org

Prussion Blue-Supported Annealing Chemical Reaction Route Synthesized Double-Shelled Fe_2O_3/Co_3O_4 Hollow Microcubes as Anode Materials for Lithium-Ion Battery

Zhaoqiang Li, Bo Li, Longwei Yin,* and Yongxin Qi

Key Laboratory for Liquid−Solid Structural Evolution and Processing of Materials, Ministry of Education, School of Materials Science and Engineering, Shandong University, Jinan 250061, P. R. China

Supporting Information

ABSTRACT: Fe_2O_3/Co_3O_4 double-shelled hierarchical microcubes were synthesized based on annealing of double-shelled $Fe_4[Fe(CN)_6]_3/Co(OH)_2$ microcubes, using $Co(AC)_2$ as a Co^{2+} source to react with OH^- generated from the reaction of ammonium hydroxide and water. The robust Fe_2O_3 hollow microcube at the inner layer not only displays a good electronic conductivity but also acts as stable supports for hierarchical Co_3O_4 outside shell consisting of nanosized particles. The double-shelled hollow structured Fe_2O_3/Co_3O_4 nanocomposites display obvious advantages as anode materials for LIBs. The hollow structure can ensure the presence of additional free volume to alleviate the structural strain associated with repeated Li^+-insertion/extraction processes, as well as a good contact between electrode and electrolyte. The robust Fe_2O_3 shell acts as a strong support for Co_3O_4 nanoparticles and efficiently prevents the aggregation of the Co_3O_4 nanoparticles. Furthermore, the charge transfer resistance can be greatly decreased because of the formation of interface between Fe_2O_3 and Co_3O_4 shells and a relative good electronic conductivity of Fe_2O_3 than that of Co_3O_4, resulting in a decrease of charge transfer resistance for improving the electron kinetics for the hollow double-shelled microcube as anode materials for LIBs. The Fe_2O_3/Co_3O_4 nanocomposite anode with a molar ratio of 1:1 for Fe:Co exhibits the best cycle performance, displaying an initial Coulombic efficiency of 74.4%, delivering a specific capacity of 500 mAh g^{-1} after 50 cycles at a current density of 100 mA g^{-1}, 3 times higher than that of pure Co_3O_4 nanoparticle sample. The great improvement of the electrochemical performance of the synthesized Fe_2O_3/Co_3O_4 double-shelled hollow microcubes can be attributed to the unique microstructure characteristics and synergistic effect between the inner shell of Fe_2O_3 and outer shell of Co_3O_4.

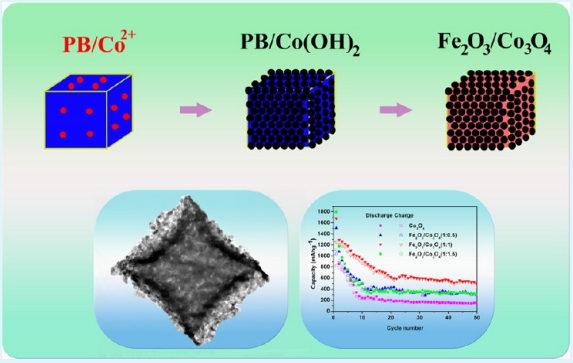

KEYWORDS: *coordination polymer, double-shelled microcubes, cobalt oxide, iron oxide, anode, lithium-ion battery*

1. INTRODUCTION

Lithium-ion batteries (LIBs) have been the most intensively used energy storage devices in recent years because of their advantages such as high energy density, high open-circuit voltage, lack of memory effects, and controllable shape.[1] LIBs are composed of three major components: cathode, anode, and electrolyte.[2] Designing electrode materials with high energy density and cycling stability is an important issue to enhance the performance of LIBs. The graphite materials are currently used anode material in commercial LIBs, exhibiting a relatively low Li storage capacity of 370 mAh g^{-1}. Thus, it has become an urgent task to search for higher capacity anode materials for the next generation LIBs.[3] Transition metal oxides have drawn much attention for their applications as anode materials for LIBs due to their low cost, wide availability, and especially higher theoretical specific capacities (>600 mAh g^{-1}).[4−7] Among the transition metal oxides, Co_3O_4 attracts extensive interest due to its high theoretical capacity (890 mAh g^{-1}), accelerating the rapid development in this field.[8] However, its large volume change during the Li^+ extraction and insertion process will lead to pulverization of the electrode materials, resulting in decrease in cycling stability and reversible capacity.[9−13]

Generally, two efficient techniques are adopted to alleviate the volume change of the electrode materials. One way is to form a buffer layer to alleviate the stress, such as carbon,[14] graphene,[15] conducting polymer,[16] ect. Another is to build a robust hierarchical hollow or porous structure to provide additional free volume to alleviate the structural strain associated with repeated Li^+-insertion/extraction processes and thus lead to an improved cycling stability.[17] Furthermore, hollow structured materials with a large interior space and a large specific area could provide sufficient contact between the electrode and the electrolyte.

Received: January 22, 2014
Accepted: May 15, 2014
Published: May 15, 2014

   dx.doi.org/10.1021/am500417j | ACS Appl. Mater. Interfaces 2014, 6, 8098−8107

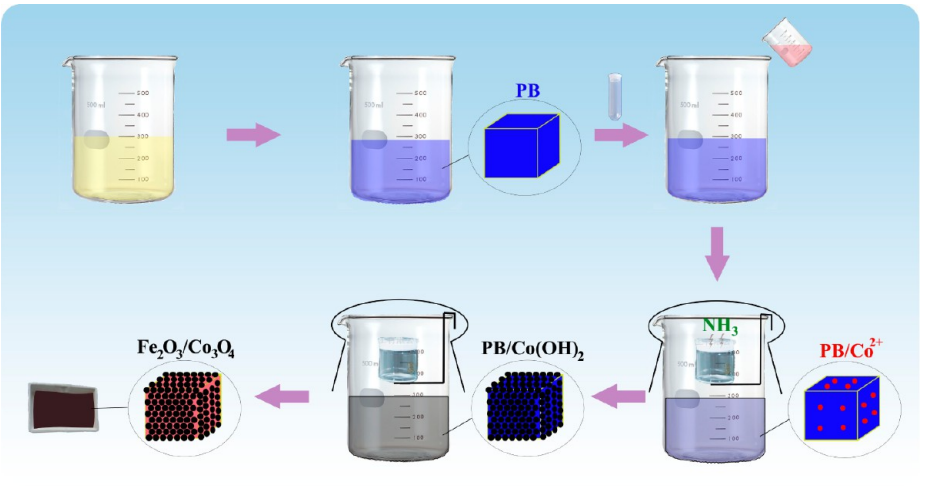

Figure 1. Schematic illustration of the synthetic process of double-shelled Fe_2O_3/Co_3O_4 hollow microcubes.

Previous reports on hollow structured materials showed excellent electrochemical performance of hollow materials as electrode for LIBs. For example, Tao et al. reported Co_3O_4 hollow microspheres with micro- and nanoscale composite structure self-assembled by nanosheets, exhibiting an improved discharge capacity as anode materials for LIBs.[18] It is reported that the hollow porous Co_3O_4, TiO_2, and SnO_2, as anode materials for LIBs with improved crystallinity and large specific surface area showed a high specific capacity and stable cycle performance.[19] Not only the hollow structured materials but also core−shell composites are regarded as promising anode materials for LIBs due to their unique microstructures that benefit the electrochemical performance in LIBs. For example, an extraordinarily high reversible capacity of SnO_2/α-MoO_3 core−shell nanobelts as anode materials for LIBs can be attributed to the presence of α-MoO_3 that could make extra Li_2O reversibly convert to Li^+.[20] Cui et al. designed a novel carbon−silicon core−shell nanowires as high power and long life LIBs anodes due to the synergistic effect between the core and shell section.[21] A unique core−shell SnO_2 nanostructured materials by Deng et al. could store an exceedingly large amount of Li^+, and exhibited improved electrochemical performance.[22] So designing core/shell structured materials with unique structure could be an effective way to improve electrochemical performance of anode materials in LIBs. Recent investigation suggests that hollow double-shelled $CoMn_2O_4$ microcubes as anodes for LIBs can retain a high discharge capacity of 624 mAh g^{-1} after 50 cycles at a current density of 200 mA g^{-1}.[23] So the design of materials with unique structure could be a effective way to obtain good anode materials with good electrochemical performance. Recently metal oxides obtanied by directly annealing coordination polymers (CPs) have been promising anode materials. Owing to the unique structures, Fe_2O_3,[24,25] Fe_3O_4,[26] CuO,[27] and Co_3O_4[19] derived from CPs exhibited good electrochemical performance for LIBs.

The electrochemical performance can be further improved by designing nanostructured materials. Compared with bulk materials, nanostructured materials have drawn much attention for their application in LIBs because of their numerous advantages, such as larger surface area, more active lithium storage sites, shorter Li^+ diffusion length, enhanced electron transportation.[28,29] However, it is known that nanostructured material electrode undergoes significant volume change during lithiation and delithiation process, which leads to breakdown of electrical pathways (the so-call pulverization) and thereafter rapid capacity fading.[29,30] Furthermore, pronounced agglomeration of nanostructured particles may inevitably take place during electrochemical cycling.[31,32] According to the diffusion formula $t = L^2/2D$ (where t is the diffusion time, L is the diffusion distance, and D is the diffusion coefficient),[33] the agglomeration of the nanomaterials can lengthen the average Li^+ diffusion path, thus results in bad performance of the electrode materials for LIBs. Some measures are proved to be successful to alleviate or even avoid the agglomeration of nanomaterials.[27,28]

Herein, we report a two-step process for the synthesis of double-shelled Fe_2O_3/Co_3O_4 hollow microcubes by a slow-chemical reaction method. The double-shelled hollow structured Fe_2O_3/Co_3O_4 nanocomposites have some advantages as anode materials for LIBs. Compared with pure Co_3O_4 sample, the hollow Fe_2O_3/Co_3O_4 (1:1) double shelled nanocomposite with a molar ratio of 1:1 for Fe/Co displays with a lower charge transfer impedance and greatly improved charge transfer ability at the interface bwetween the anode and the electrolyte.

2. EXPERIMENTAL SECTION

2.1. Synthesis of the Prussion Blue Microcubes. The Prussion blue (PB) microcubes were synthesized according to a previous work.[24] Briefly, polyvineypirrolydone (PVP, K30, MW ≈ 40 000, 22.8 g) were dissolved in a HCl solution (0.1 M, 300 mL) and we obtained a transparent solution. Then 0.66g $K_4Fe(CN)_6{\cdot}3H_2O$ were added to this solution under magnetic stirring. After 30 min, the obtained clear pale yellow solution was transferred into a bottle, which was then placed into an electric oven and heated at 80 °C for 24 h. The obtained blue liquid was filtered and washed several times with deionized water and absolute ethanol for several times. Finally, we obtained the PB microcubes.

2.2. Synthesis of the Co_3O_4/Fe_2O_3 Composites. Typically, the obtained PB mirocubes was dispersed in a mixture which contained a certain amount of $Co(AC)_2{\cdot}3H_2O$, 1.6 g of PVP, 16 mL of alcohol, and 35 mL of H_2O. The mixture was homogeneously mixed by magnetic stirring and ultrasonication and then put into a beaker with ammonium hydroxide dangling in it. Then the resulting mixture was stirred for 12 h at 80 °C. The obtained black product was filtered and washed several times with distilled water and absolute ethanol and finally dried in a vacuum oven at 35 °C for 12 h. To obtain the final product, the as-synthesized black product was heated at 650 °C with a temperate ramp of 2 °C min^{-1} for 6 h in air.

dx.doi.org/10.1021/am500417j | ACS Appl. Mater. Interfaces 2014, 6, 8098−8107

2.3. Materials Characterization. X-ray diffraction (XRD) patterns were collected using Rigaku D/Max-Rb diffractometer equipped with Cu Ka radiation(λ = 1.5406 Å). The morphology and components of the synthesized products were analyzed using SU-70 field emission scanning electron microscopy (FE-SEM) and attached X-ray energy dispersive spectrometry (EDS), respectively. The morphology and structure of the synthesized products were analyzed using high-resolution transmission electron microscopy (HR-TEM) of JEM-2100 at an acceleration voltage of 200 kV Nitrogen adsorption−desorption isotherms were determined at 77 K using Gold APP V-Sorb 2800P surface area and porosity 60 analyzer. The surface area measurements were performed according to the Brunauer−Emmett−Teller (BET) method. The pore size distribution was obtained from the adsorption branch of the isotherm using the Kelvin equation by means of the Barrett−Joyner−Halenda (BJH) method.

2.4. Electrochemical Measurements. The electrochemical measurements were carried out by using 2032 coin-type cells, which contain the Fe_2O_3/Co_3O_4 composite material as negative electrode, a cellgard 2325 as separator, a lithium metal foil as reference electrode and a solution of 1.0 M $LiPF_6$ in mixed ethylene carbonate (EC) and diethyl carbonate (DEC) (EC/DEC, 1:1 by volume) as the electrolyte. The working electrode is composed of Fe_2O_3/Co_3O_4 composites, polyvinylidene difluoride (PVDF) and acetylene black in a weight ratio of 70:15:15. The cells were assembled in an Ar-filled glovebox. Charge/discharge test of the cells was performed in potential range of 3.00−0.01 V on a LAND CT2001A battery test system (Wuhan, China) at room temperature. The cyclic voltammetry (CV) study was conducted using an electrochemical workstation (PARSTAT 2273) between 3.00 and 0.01 V at a scan rate of 0.1 mV s^{-1}.

3. RESULTS AND DISCUSSION

The schematic illustration for the synthetic process of double-shelled Fe_2O_3/Co_3O_4 hollow microcubes is shown in Figure 1. After the synthesis of prussion blue (PB) mirocubes, they were dispersed into a PVP solution. Then Co^{2+} ions were connected to the surface of PB mircocubes after the introduction of $Co(AC)_2$. Under 80 °C, the NH_3 was released slowly from the ammonium hydroxide and then dissolved in the solution to produce OH^-. The slow reaction between Co^{2+} and OH^- leads to the formation of nanosized $Co(OH)_2$ shell on surface of the PB microcubes. The reactions are described as

$$NH_3 + H_2O \rightarrow NH_4^+ + OH^- \quad (1)$$

$$Co^{2+} + 2OH^- \rightarrow Co(OH)_2 \quad (2)$$

An annealing treatment was carried out at 650 °C for 6 h in air with a ramping rate of 2 °C min^{-1}, the $PB/Co(OH)_2$ microcubes were transformed into Fe_2O_3/Co_3O_4 hollow microcubes.

Figure 2 depicts the powder X-ray diffraction (XRD) patterns of the Fe_2O_3/Co_3O_4 nanocomposites with different contents of Co_3O_4 incorporated, with a molar ratio of 1:0.5, 1:1 and 1:1.5 for Fe:Co, respectively. The XRD patterns of the synthesized nanocompistes display the similar diffraction peaks, which can be indexed to standard cubic Co_3O_4 (JCPDS 42-1467), cubic bixbyite β-Fe_2O_3 (JCPDS 39-0238), and cubic spinel γ-Fe_2O_3 (JCPDS 39-1346), indicating that the synthesized nanocomposites are composed of Fe_2O_3 and Co_3O_4 phases. From the XRD patterns in Figure 2, it is shown that with the content of Co_3O_4 incorporated increasing, the diffraction peaks related to Co_3O_4 phase gets stronger. To make a comparison of the electrochemical performance between the Fe_2O_3/Co_3O_4 nanocomposites and pure Co_3O_4, the pure Co_3O_4 nanoparticles were also synthesized, of which XRD pattern is given in Figure S1 in Supporting Information.

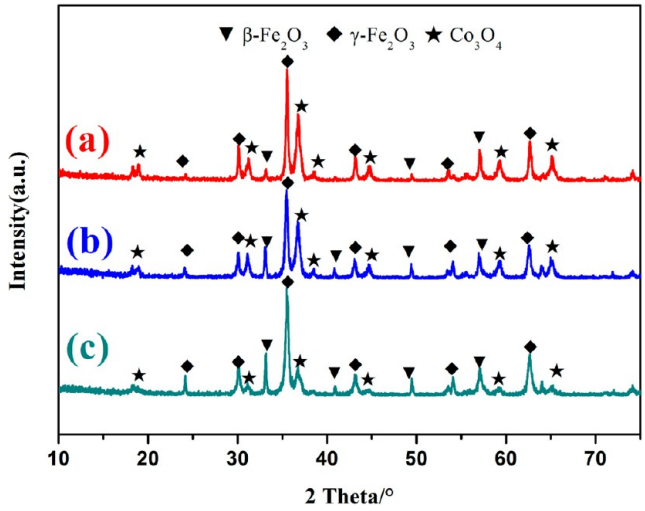

Figure 2. Wide-angle XRD patterns of the Fe_2O_3/Co_3O_4 hollow microcubes with a molar ratio of (a) 1:0.5, (b) 1:1, and (c) 1:1.5, respectively.

Field emission scanning electron microscopy (FE-SEM) examination was carried out to elucidate the morphology and microstructure of the synthesized Fe_2O_3/Co_3O_4 composites. From Figure 3a, it is indicated that the synthesized PB

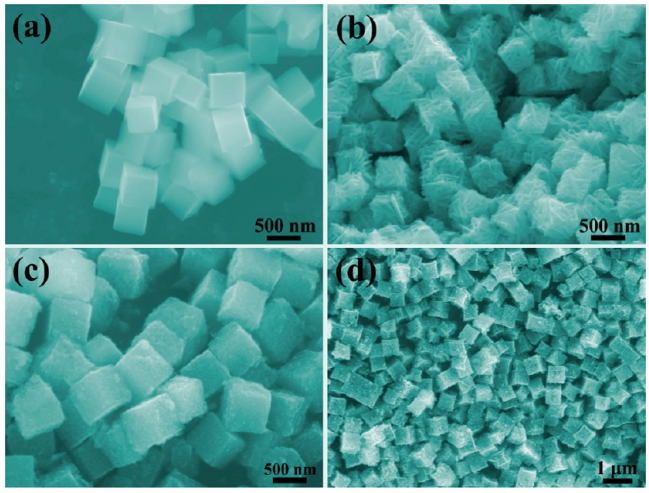

Figure 3. FE-SEM images of (a) Prussion Blue microcubes, (b) Fe_2O_3 microcubes transformed from PB, (c) $PB/Co(OH)_2$ microcubes, and (d) Fe_2O_3/Co_3O_4 (Fe:Co: 1:1) hollow microcubes.

microcubes display a smooth surface with a highly uniform morphology with an average size of ~800 nm. After calcination treatment at 650 °C for 6 h, the smooth PB microcubes transformed to robust Fe_2O_3 microcubes, retaining their original cube-like morphology of PB microcubes, as shown in Figure 3b. When the reaction solution of $Co(AC)_2$ was mixed with PB microcubes in advance (according to different atomic ratio for Fe/Co of 1:0.5), the synthesized microcubes show a relatively rough surface compared with smooth surface of PB microcubes (Figure 3c), indicating the formation of the $PB/Co(OH)_2$ (Fe/Co = 1:0.5) nanocomposite with a thin layer of $Co(OH)_2$ deposited on the outer surfaces of PB. After calcination at 650 °C for 6 h, the $PB/Co(OH)_2$ microcubes transformed into uniform porous microcubes of Fe_2O_3/Co_3O_4 (Fe/Co: 1:0.5) (Figure 3d).

dx.doi.org/10.1021/am500417j | ACS Appl. Mater. Interfaces 2014, 6, 8098−8107

Figure 4 comparatively illustrates the detail microstructures of Fe_2O_3/Co_3O_4 microcube nanocomposites with different

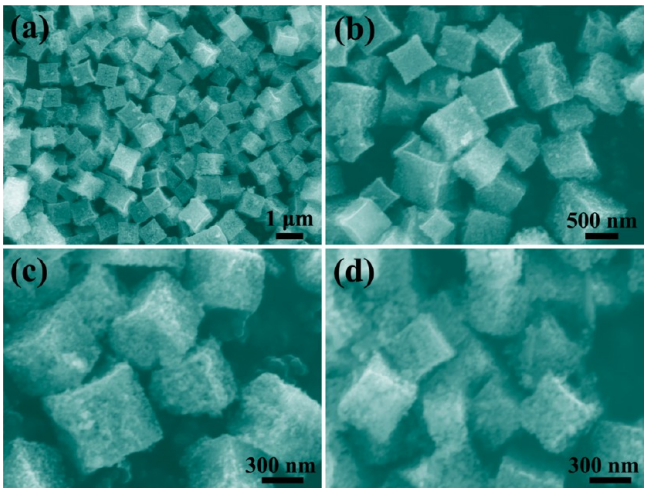

Figure 4. FE-SEM images of Fe_2O_3/Co_3O_4 hollow double-shelled microcubes with different molar ratio of Fe/Co: (a) 1:0.5, (b,c) 1:1, and (d) 1:1.5, respectively.

molar ratio of 1:0.5 (Figure 4a), 1:1 (Figure 4b, c), and 1:1.5 (Figure 4d) for Fe/Co. For the outer layer of Co_3O_4, the high magnification SEM images of Fe_2O_3/Co_3O_4 microcubes show that the outer shell is consisted of Co_3O_4 nanoparticles of 20–30 nm. With the content of Co_3O_4 increasing, the Fe_2O_3 inner shell tends to distort. As the content of Co_3O_4 achieves a value of a molar ratio of 1:1.5 for Fe/Co, the Fe_2O_3 inner shell almost collapses.

For the chemical composition component and elemental distribution of the double-shelled microcube nanocomposites, EDS analysis shows that the nanocomposites are composed of Fe, Co, and O elements. Figure 5 gives a typical EDS elemental

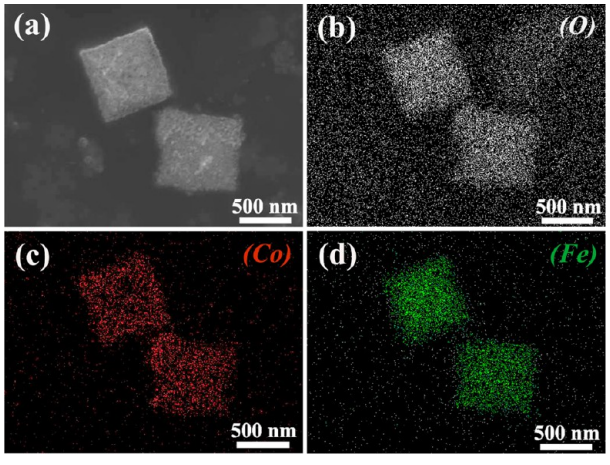

Figure 5. (a) SEM image (b) O, (c) Co, and (d) Fe elemental mapping images of Fe_2O_3/Co_3O_4 hollow microcubes.

mapping analysis of the Fe_2O_3/Co_3O_4 (1:1) microcube sample, evidently revealing the homogeneous distribution of Fe, Co and O among the whole nanocompoiste microcubes. It is can be concluded that uniform Fe_2O_3/Co_3O_4 double-shelled microcubes were successfully synthesized by a slowly chemical reaction method. It is clearly indicated that the Fe_2O_3 layer is at inner shell and the Co_3O_4 shell is on the outer side of the Fe_2O_3/Co_3O_4 nanocomposite.

Transmission electron microscopy is used to further reveal the detailed microstructures of the Fe_2O_3/Co_3O_4 microcubes. Uniform microcubes with an average size of 800 nm are revealed in the low-resolution TEM images of the synthesized Fe_2O_3/Co_3O_4 products with different Fe:Co ratio of 1:0.5 (Figure 6a–c) and 1:1 (Figure 6d, f), in agreement well with the SEM results described above. Hollow structure nature of the microcubes is clearly shown in the TEM images, with a shell of Fe_2O_3 inside and the Co_3O_4 layer on the shell outside, corresponding to the result obtained via the examination of EDS elemental mapping. Moreover, it can be seen that the outer shell of Co_3O_4 is composed of nanoparticles of 20–30 nm (Figure 6g), which is consistent with the SEM observations. The marked *d*-spacing of 0.25 nm in a high-resolution TEM lattice image of an individual Co_3O_4 nanoparticle (Figure 6h) corresponds well to the *d*-spacing of (311) plane of Co_3O_4 (JCPDS No. 42-1467). The diffraction rings in a selected area electron diffraction (ED) pattern (Figure 6i) match well with (220), (440), (311) planes of γ-Fe_2O_3, and (311) planes of Co_3O_4 and (440) plane of β-Fe_2O_3. This is in correspondence well with the XRD characterization results.

The nitrogen adsorption–desorption isotherms and pore size distribution curves by the Barrett–Joyner–Halenda (BJH) method of the simple Co_3O_4 nanoparticles and Fe_2O_3/Co_3O_4 (1:1) hollow microcubes are shown in Figure 7. The two isotherms are similar to each in form, exhibiting a typical type IV with a type H1 hysteresis loop, indicating the presence of the mesopores.[34] The hysteresis loop shown in isotherms is very narrow and small, suggesting the presence of macropores in the samples.[35] Table 1 gives the important structural parameters derived from the nitrogen adsorption and desorption isotherms of the samples. The specific surface area of the Fe_2O_3, Co_3O_4, and Fe_2O_3/Co_3O_4 (1:1) composite is 22.5, 28.5, and 30.5 $m^2\ g^{-1}$, respectively. The Fe_2O_3/Co_3O_4 (1:1) composites exhibit higher surface area than pure Co_3O_4 nanoparticles, indicating that the transformation of the simple Co_3O_4 nanoparticles to hierarchical Co_3O_4 shell led to an increase in the surface area. The unique double-shelled Fe_2O_3/Co_3O_4 microcube-like structures with complicated hierarchical Co_3O_4 shell made an increase in both the specific surface area and the total pore volume, permitting the electrolyte to easily penetrate through the electrode, which would be useful for the enhancement of electrochemical performance as anode materials for LIBs.

To understand the redox reactions of the synthesized Fe_2O_3/Co_3O_4 composite, the CV curves for the first three cycles of the Fe_2O_3/Co_3O_4 composite were investigated at a scan rate of 0.1 mV s^{-1} in the voltage range of 3.00–0.01 V versus Li^+/Li (Figure 8). In the first cycle, two cathodic peaks located at 0.5 and 0.75 V were observed for the Fe_2O_3/Co_3O_4 composite electrode. The bulky peaks at 0.5 V can be attributed to the reduction of Fe^{3+} to Fe^0 and the irreversible reaction related to the formation of SEI.[36] The other tiny peak at 0.75 V possibly because of the multistep electrochemical reduction (lithiation) reaction o f Co_3O_4 with Li.[37] Two obvious anodic peaks located at 1.75 and 2.2 V were observed in the first anodic scan. The anodic peak located at 1.75 V may attributed to the reversible oxidation of Fe^0 to Fe^{3+} during the charge process.[38] Another anodic peak located at 2.2 V may be ascribed to the oxidation (delithiation) reaction of Co_3O_4.[39]

dx.doi.org/10.1021/am500417j | ACS Appl. Mater. Interfaces 2014, 6, 8098–8107

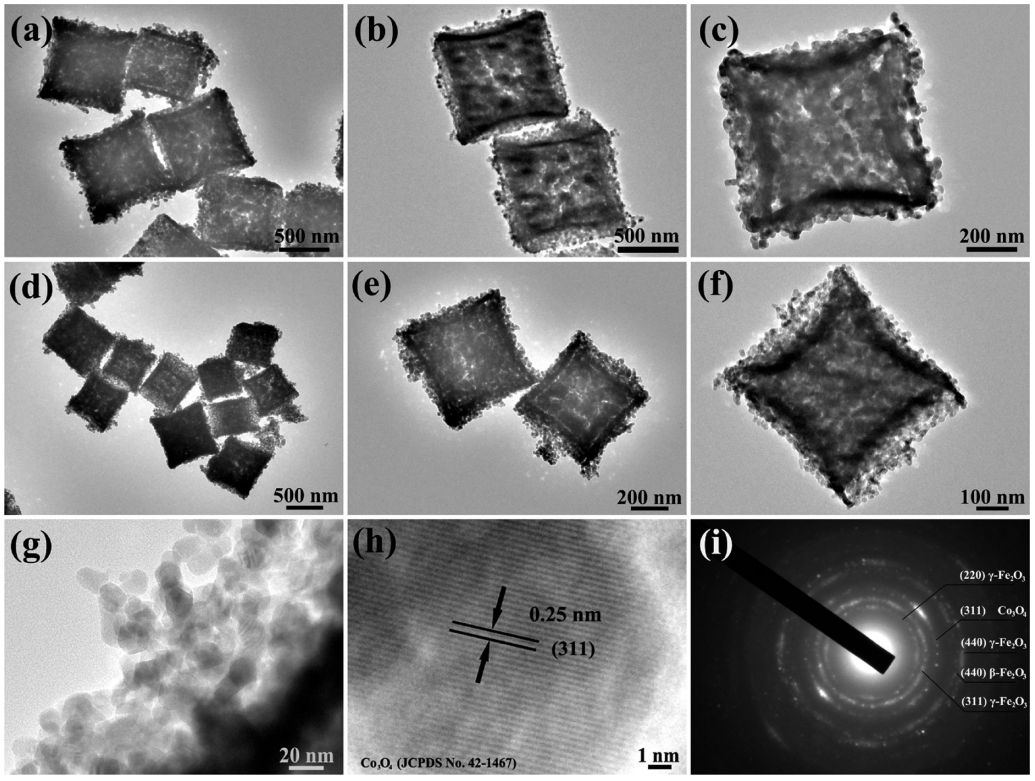

Figure 6. TEM images of Fe_2O_3/Co_3O_4 (1:0.5) hollow microcubes with different molar ratio for Fe/Co: (a–c) 1:0.5 and (d–f) 1:1. (g) TEM image of Co_3O_4 hierarchical shell. (h) High resolution TEM lattice image of a Co_3O_4 nanoparticle. (i) SAED patterns of the Fe_2O_3/ Co_3O_4 (1:1) samples.

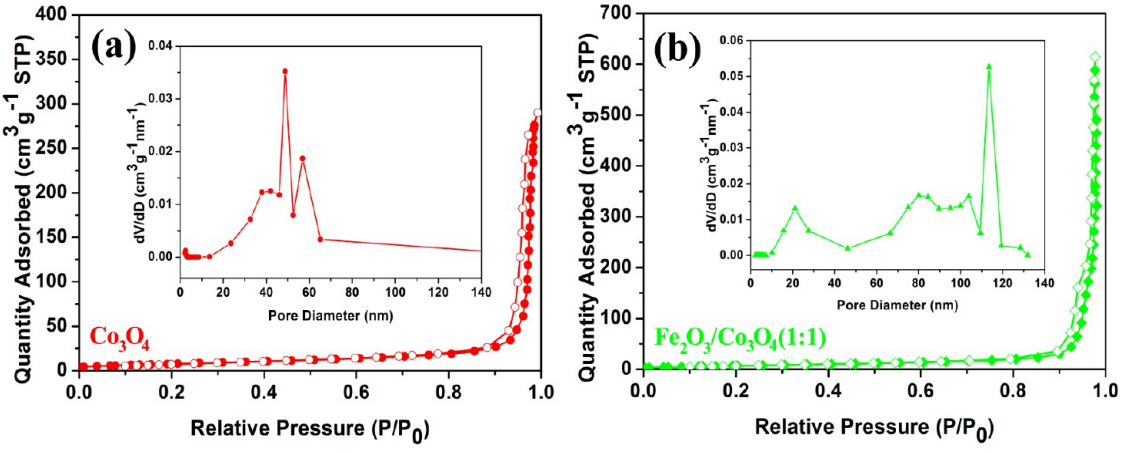

Figure 7. N_2 adsorption–desorption isotherms and pore size distributions (inset) of (a) Co_3O_4 and (b) Fe_2O_3/Co_3O_4 (1:1) samples.

Table 1. Textural Parameters of the Fe_2O_3, Co_3O_4, and Fe_2O_3/Co_3O_4 Composites

sample	BET surface area ($m^2\ g^{-1}$)	pore diameter (nm)	total pore volume ($cm^3\ g^{-1}$)
Fe_2O_3	22.5	71	1.04
Co_3O_4	28.5	43	0.46
Fe_2O_3/Co_3O_4 (1:0.5)	26.0	48	1.00
Fe_2O_3/Co_3O_4 (1:1)	30.5	53	0.90
Fe_2O_3/Co_3O_4 (1:1.5)	32.3	38	0.59

In the second cycle, we can observe the obvious decrease in the peak intensity and integral area, which resulted from the irreversible capacity caused by the formation of SEI. Compared with the first cathodic scan, the main cathodic peaks shifted to 0.8 V for Fe_2O_3 and 1.2 V for Co_3O_4.[17] The significant difference in the lithiation voltage may be related to the changes of the Fe_2O_3 and Co_3O_4 interfacial property.[40] The peak intensity and integral areas of the third cycle are close to that of the second one for Fe_2O_3/Co_3O_4 composite electrode, indicating the good electrochemical reversibility of Fe_2O_3/Co_3O_4 composite. The formation of Co(Fe) and Li_2O and the reformation of $Co_3O_4(Fe_2O_3)$ can be described by the below electrochemical conversion reaction:

$$Co_3O_4 + 8Li^+ \Leftrightarrow 4Li_2O + 3Co \quad (3)$$

$$Fe_2O_3 + 6Li^+ \Leftrightarrow 3Li_2O + 2Fe \quad (4)$$

dx.doi.org/10.1021/am500417j | ACS Appl. Mater. Interfaces 2014, 6, 8098–8107

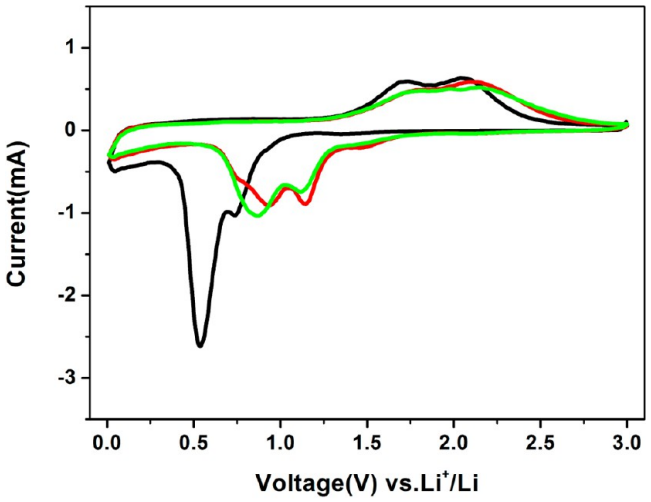

Figure 8. CV curves of the Fe_2O_3/Co_3O_4 electrode for three cycles at a scan rate of 0.1 mV s^{-1} in the voltage range of 3.00−0.01 V.

Figure 9 shows the Nyquist profiles of the AC impedance for the Co_3O_4 nanoparticles, Fe_2O_3 microcubes, and Fe_2O_3/Co_3O_4

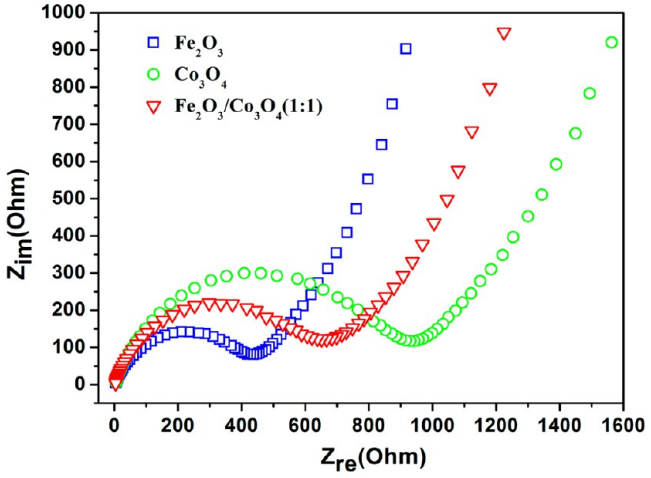

Figure 9. Nyquist plot of the simple Co_3O_4 nanoparticles, Fe_2O_3 microcubes, and Fe_2O_3/Co_3O_4 (1:1) hollow microcubes.

(1:1) hollow microcubes, which were measured at an open circuit voltage state using fresh cells. Each plot consists of a semicircle in the high-frequency region that attributed to the charge transfer process, and a sloping line in the low-frequency region that related to the mass transfer of lithium ions. The Nyquist plots for the three samples were similar in shape except for the diameters of the semicircles, and thereby the associated impedance values.[41] Compared with EIS spectrum of pure Co_3O_4 nanopartile sample, the EIS spectra of Fe_2O_3 and Fe_2O_3/Co_3O_4 (1:1) hollow microcubes display relatively smaller diameters, indicating a lower impedance value of the Fe_2O_3 and Fe_2O_3/Co_3O_4 (1:1) hollow microcubes. So the charge transfer of Fe_2O_3/Co_3O_4 hollow microcube electrode is easier than that of pure Co_3O_4 nanoparticle sample, thus leading to a better electrochemical performance for the Fe_2O_3/Co_3O_4 hollow microcubes than pure Co_3O_4 nanoparticle sample.

The relatively lower charge transfer resistance of Fe_2O_3/Co_3O_4 hollow microcubes than the pure Co_3O_4 nanoparticles resulted from the formation of interface between Fe_2O_3 and Co_3O_4 shells, and a relative good electronic conductivity of Fe_2O_3 than that of Co_3O_4. The charge transfer enhancement mechanism of the Fe_2O_3/Co_3O_4 double-shell microcubes is depicted in Figure 10. For the electrode of pure Co_3O_4

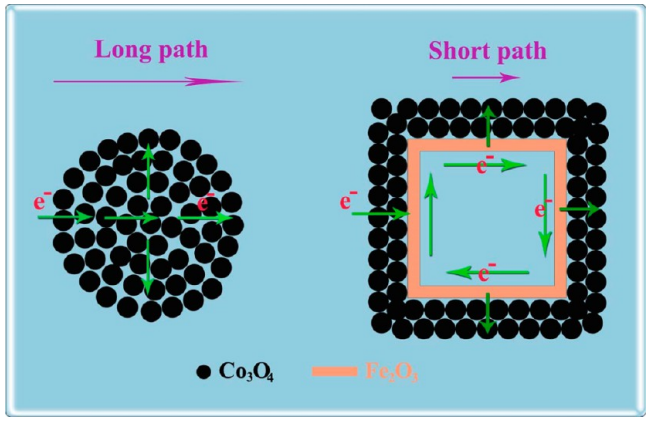

Figure 10. Charge transfer enhancement mechanism of the double-shell microcubes.

nanoparticles, the electrons are transferred from one nanoparticle to another with a slow speed for a long path. While for the electrode of Fe_2O_3/Co_3O_4 hollow composite microcubes, the electrons are first transferred from Co_3O_4 nanoparticels to Fe_2O_3 hollow shell with a shorter path because of the interface formation between Co_3O_4 and Fe_2O_3 double shell hollow structure. Once transferred to Fe_2O_3 hollow shell, the electrons can spread quickly to the other Co_3O_4 nanoparticles adhered closely to the Fe_2O_3 hollow shell because of the relatively good electrical conductivity of Fe_2O_3 than that of Co_3O_4. So the formation of the double-shelled Fe_2O_3/Co_3O_4 composites promotes the transfer ability of electrons to a certain extent in the electrode, leading to a lower charge transfer resistance of Fe_2O_3/Co_3O_4 hollow microcubes than pure Co_3O_4 nanoparticles. Such phenomenon is also found in previously reported work on the related core−shell structures, in which inner cores with better conductivity can lead to a better electron transfer ability, and homogeneous electrochemical accessibility and high ionic conductivity by avoiding agglomeration.[42−44]

Galvanostatic discharge−charge (Li insertion−extraction) experiments were carried out to evaluate the electrochemical performance of the Fe_2O_3/Co_3O_4 (1:1) composite and pure Co_3O_4 nanoparticle electrodes at a current density of 100 mA g^{-1} between 3.00 and 0.01 V vs Li^+/Li. Figure 11 shows profiles for the voltage versus capacity of the first, second and fifth cycle of the synthesized samples. For the pure Co_3O_4 electrode, the first discharge and charge capacity are 1113 and 826 mAh g^{-1}, corresponding to an initial Coulombic efficiency of 74.2%. But the capacity dropt rapidly during the cycle processes. At the fifth cycle, the discharge and charge capacity are 714 and 556 mAh g^{-1}, respectively, only 50% retention of the initial discharge capacity. For the Fe_2O_3/Co_3O_4 (1:1) composite, the first discharge and charge capacities are 1687 and 1249 mAh g^{-1}, respectively, with a greatly enhancement of the cycling stability and capacity enhancement. The initial Coulombic efficiency is as high as 74.4%. The capacity loss in the subsequent cycles is slower than the simple Co_3O_4, indicating a better electrochemical performance of the

dx.doi.org/10.1021/am500417j | ACS Appl. Mater. Interfaces 2014, 6, 8098−8107

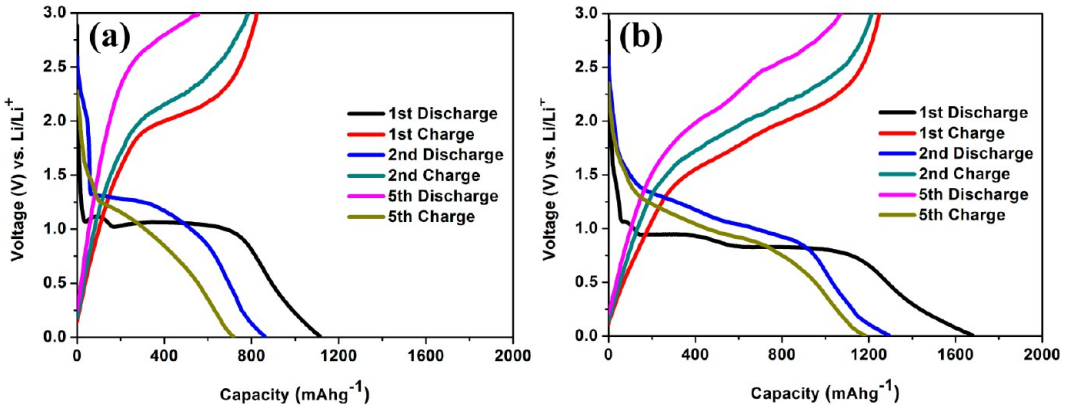

Figure 11. Discharge−charge profiles of electrode at a current density of 100 mA g^{-1} in the voltage range 3.00−0.01 V versus Li^+/Li: (a) pure Co_3O_4 nanoparticles and (b) the Fe_2O_3/Co_3O_4 (1:1) hollow microcubes.

composite. In the first-discharge curve, the potential quickly falls to a 0.8 V plateau and then gradually declines to the cutoff voltage of 0.01 V. This is consistent with CV result, ascribed to the lithiation reaction of Fe_2O_3/Co_3O_4 and irreversible formation of SEI film. This plateau shifted up to 1.2 V in the second discharge curve. The plateau at 1.75−2.2 V can be ascribed to the delithiation of electrode. The result above agreed well with the CV result.

Figure 12 comparatively describes the cycle performance and stability of the prepared double-shelled Fe_2O_3/Co_3O_4 micro-

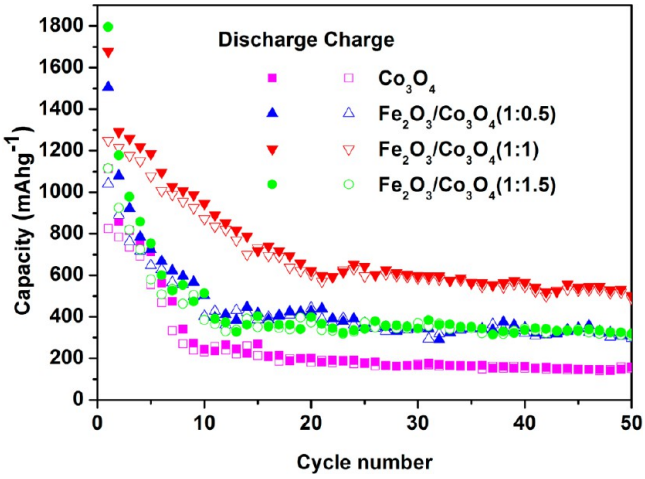

Figure 12. Discharge and charge capacity vs cycle numbers curves of the Fe_2O_3/Co_3O_4 and pure Co_3O_4 electrodes cycled at a current density of 100 mA g^{-1} in the voltage range 3.00−0.01 V versus Li^+/Li for 50 cycles.

cubes and the pure Co_3O_4 nanoparticles as anode materials at a current density of 100 mA g^{-1} between 3.00 and 0.01 V at room temperature. For comparison, we also studied the cycle performance of the pure Fe_2O_3, as is shown in Supporting Information Figure S3. The synthesized pure Fe_2O_3 microcubes can deliver a discharge and charge capacity of 1108/806 mAh g^{-1} maintainance during the first lithiation and delithiation process, corresponding to an initial Coulombic efficiency of 72.8%. After 50 cycles, the pure Fe_2O_3 sample delivers a reversible capacity of 443 mAh g^{-1} at a current density of 100 mA g^{-1}. In the first 10 cycles, the Coulombic efficiency of pure Co_3O_4 nanoparticle sample even did not exceed 91%, and the discharge capacity dropt quickly from 1113 to about 240 mAh g^{-1}. At the 50th cycle, it can only maintain a capacity of 150 mAh g^{-1}, showing a bad cycle performance for the pure Co_3O_4 nanoparticle sample. However, double-shelled Fe_2O_3/Co_3O_4 composites showed better cycle performance as anode materials for LIBs. The first discharge/charge capacity of the Fe_2O_3/Co_3O_4 (1:0.5, 1:1 and 1:1.5) is 1505/1040, 1678/1249, and 1796/1116 mAh g^{-1}, corresponding to an initial Coulombic efficiency of 69.1%, 74.4%, and 62.2%, respectively, with a greatly capacity enhancement compared with pure Co_3O_4 nanoparticle sample. Among all the composites, the Fe_2O_3/Co_3O_4 (1:1) anode exhibits the best cycle performance. At the current density of 100 mA g^{-1}, the Coulombic efficiency of the second cycle can reach 94%. The discharge capacity exhibits a slow capacity loss in the first 20 cycles and it can still maintain 650 mAh g^{-1} at the 20th cycle. After 50 discharge and charge processes, it can still delivered a specific capacity of 500 mAh g^{-1}. For the Fe_2O_3/Co_3O_4 (1:1) composite, the mass ratio of the two active material is calculated as 1:1. So taking the capacity contribution of 221 mAh g^{-1} for the Fe_2O_3 (443 mAh g^{-1} for pure Fe_2O_3) into account in the doubel-shlled Fe_2O_3/Co_3O_4 composites, the capacity of the Co_3O_4 hierarchical shell is 558 mAh g^{-1}, which is more than 3 times of pure Co_3O_4 nanoparticle sample in the present work.

Rate capabilities of the Fe_2O_3/Co_3O_4 (1:1) double-shelled microcubes and the pure Co_3O_4 under various current densities from 100 to 800 mA g^{-1} are shown in Figure 13. For comparison, the rate capability of the pure Fe_2O_3 hollow microcubes is also shown in Supporting Information Figure S3b. As is shown above, the pure Co_3O_4 nanoparticles can only deliver 220, 162, and 120 mAh g^{-1} at the current density of 200, 400, and 800 mA g^{-1}, respectively, which displayed a bad rate capability. However, the double-shelled microcubes showed much better rate performance under the same condition. It can deliver 738 and 456 mAh g^{-1} when cycled at 200 and 400 mA g^{-1}. Even at the high current density of 800 mA g^{-1}, it can still retain 272 mAh g^{-1}, which is better than the pure Co_3O_4 nanoparticles (120 mAh g^{-1}) and the pure Fe_2O_3 hollow microcubes (238 mAh g^{-1}). Furthermore, the capacity can recover to 690 mAh g^{-1} when the current density reduced to 100 mA g^{-1}, indicating good rate capability of the Fe_2O_3/Co_3O_4 (1:1) double-shelled microcubes.

The great improvement of the electrochemical performance of the synthesized Fe_2O_3/Co_3O_4 double-shelled hollow microcubes can be attributed to the unique microstructure characteristics and synergistic effect between the inner shell

dx.doi.org/10.1021/am500417j | ACS Appl. Mater. Interfaces 2014, 6, 8098−8107

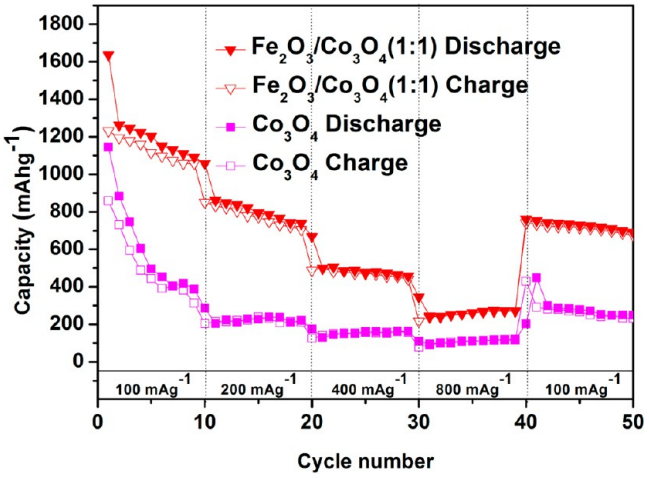

Figure 13. Rate capability of the Fe_2O_3/Co_3O_4 and pure Co_3O_4 electrodes cycled at different current densities from 100 to 800 mA g^{-1} in the voltage range 3.00−0.01 V versus Li^+/Li for 50 cycles.

of Fe_2O_3 and outer shell of Co_3O_4. The hollow structure can ensure the presence of additional free volume to alleviate the structural strain associated with repeated Li^+ insertion/extraction processes, as well as a good contact between electrode and electrolyte. The robust Fe_2O_3 hollow microcubes not only displays good electronic conductivity but also acts but also acts as a strong support for Co_3O_4 nanoparticles and can efficiently prevent the aggregation of the Co_3O_4 nanoparticles. Figure 14a and b depicts FESEM images of double-shelled

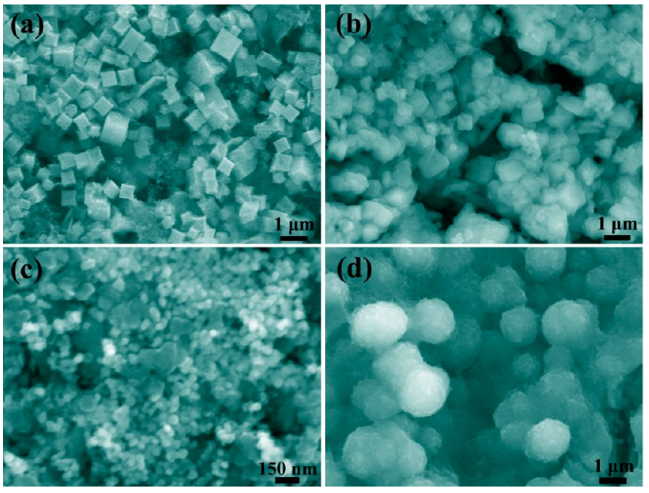

Figure 14. FE-SEM images of Fe_2O_3/Co_3O_4 microcubes working electrodes (a) before cycling and (b) after 10 cycles; FE-SEM images of pure Co_3O_4 nanoparticles working electrodes (c) before cycling and (d) after 10 cycles.

Fe_2O_3/Co_3O_4 hollow microcubes as anode materials before and after 10 cycles. After 10 cycles, no obvious change of the cubic structure for Fe_2O_3/Co_3O_4 hollow microcubes can be seen from Figure 14b, and no obvious agglomeration of the Co_3O_4 nanoparticles takes place. So the structural instability and agglomeration of the Co_3O_4 nanoparticles can be successfully alleviated by loading Co_3O_4 nanoparticles on the robust Fe_2O_3 hollow microcube. In contrast, for pure Co_3O_4 nanoparticle samples, after 10 discharge and charge cycles, the agglomeration takes place, and the nanosized Co_3O_4 nanoparticles transform to big particles with a size of 1.5 μm (Figure 14c, d). Furthermore, EIS analysis (Figure 9) shows that the charge transfer resistance of Fe_2O_3/Co_3O_4 is much lower than that of pure Co_3O_4 sample. This improvement can be attributed to relative good electronic conductivity of Fe_2O_3 than Co_3O_4, and the formation of interface between Fe_2O_3 and Co_3O_4 shells and double-shelled microcube/electrolyte interface, resulting in a decrease of charge transfer resistance for improving the electron kinetics in the electrode material, and hence, enhancing the electrochemical performance of Fe_2O_3/Co_3O_4 electrode for LIBs. The hollow Fe_2O_3/Co_3O_4 (1:1) double-shelled nanocomposite with proper amount of Co_3O_4 nanoparticles has a more stable structure and displays a lower charge transfer impedance and greatly improved charge transfer ability at the interface between the anode and the electrolyte.

4. CONCLUSIONS

In summary, we successfully synthesized double-shelled hollow microcubes by a Prussion Blue-supported slow chemical reaction method, with the robust Fe_2O_3 hollow microcubes inside and hierarchical Co_3O_4 shell outside. The great improvement of the electrochemical performance of the synthesized Fe_2O_3/Co_3O_4 double-shelled hollow microcubes can be attributed to the unique microstructure characteristics and synergistic effect between the inner shell of Fe_2O_3 and outer shell of Co_3O_4. The robust Fe_2O_3 hollow structure not only displays good electronic conductivity but also acts as a strong support of the whole structure, and Co_3O_4 nanoparticles load on the Fe_2O_3 to form a hierarchical shell, efficiently preventing the aggregation of the Co_3O_4 nanoparticles. Furthermore, EIS analysis shows that the charge transfer resistance of Fe_2O_3/Co_3O_4 is much lower than that of pure Co_3O_4 sample, hence enhancing the electrochemical performance of Fe_2O_3/Co_3O_4 electrode for LIBs. The Fe_2O_3/Co_3O_4 nanocomposite anode with a molar ratio of 1:1 for Fe:Co exhibits the best cycle performance, displaying an initial Coulombic efficiency of 74.4%, delivering a specific capacity of 500 mAh g^{-1} after 50 cycles at a current density of 100 mA g^{-1}, 3 times higher than that of pure Co_3O_4 nanoparticle sample. The novel Fe_2O_3/Co_3O_4 double-shelled microcubes should be promising high-performance anode materials for LIBs, and the slow chemical reaction method could also be extended to synthesis of other novel structures.

■ ASSOCIATED CONTENT

Ⓢ Supporting Information

Wide-angle XRD patterns of the simple Co_3O_4 nanoparticles, FE-SEM images of pure Co_3O_4 nanoparticles synthesized by the slow chemical reaction method, element content of the Fe_2O_3/Co_3O_4 microcubes measured by EDS, and cycle performance and rate performance of the Fe_2O_3 microcubes. This material is available free of charge via the Internet at http://pubs.acs.org.

■ AUTHOR INFORMATION

Corresponding Author

*Tel.: + 86 531 88396970. Fax: + 86 531 88396970. E-mail: yinlw@sdu.edu.cn.

Notes

The authors declare no competing financial interest.

■ ACKNOWLEDGMENTS

We acknowledge support from the National Natural Science Funds for Distinguished Young Scholars (51025211), National Nature Science Foundation of China (No. National Nature Science Foundation of China (no. 51272137), the Shandong Natural Science Fund for Distinguished Young Scholars (JQ200915), and the Tai Shan Scholar Foundation of Shandong Province.

■ REFERENCES

(1) Tarascon, J.-M.; Armand, M. Issues and Challenges Facing Rechargeable Lithium Batteries. *Nature* **2001**, *414*, 359−367.
(2) Lee, K. T.; Cho, J. Roles of Nanosize in Lithium Reactive Nanomaterials for Lithium Ion Batteries. *Nano Today* **2011**, *6*, 28−41.
(3) Chen, J. S.; Archer, L. A.; Lou, X. W. SnO_2 Hollow Structures and TiO_2 Nanosheets for Lithium-Ion Batteries. *J. Mater. Chem.* **2011**, *21*, 9912−9924.
(4) Hu, J. S.; Zhong, L. S.; Song, W. G.; Wan, L. J. Synthesis of Hierarchically Structured Metal Oxides and Their Application In Heavy Metal Ion Removal. *Adv. Mater.* **2008**, *20*, 2977−2982.
(5) Hyun, W. S.; Yun, H. J.; Seung, D. S.; Seung, H. L.; Dong, W. K. Highly Reversible Lithium Storage In *Bacillus subtilis*-Directed Porous Co_3O_4 Nanostructures. *ACS Nano* **2011**, *5*, 443−449.
(6) Poizot, P.; Laruelle, S.; Grugeon, S.; Dupont, L.; Tarascon, J.-M. Nano-Sized Transition-Metal Oxides As Negative-Electrode Materials for Lithium-Ion Batteries. *Nature* **2000**, *407*, 496−499.
(7) Wang, B.; Chen, J. S.; Wu, H. B.; Wang, Z.; Lou, X. W. Quasiemulsion-Templated Formation of Alpha-Fe_2O_3 Hollow Spheres with Enhanced Lithium Storage Properties. *J. Am. Chem. Soc.* **2011**, *133*, 17146−17148.
(8) Liu, J.; Xia, H.; Lu, L.; Xue, D. Anisotropic Co_3O_4 Porous Nanocapsules Toward High-Capacity Li-Ion Batteries. *J. Mater. Chem.* **2010**, *20*, 1506−1510.
(9) Yang, S. B.; Cui, G. L.; Pang, S. P.; Cao, Q.; Kolb, U.; Feng, X. L.; Maier, J.; Mullen, K. Fabrication of Cobalt and Cobalt Oxide/Graphene Composites: Towards High-Performance Anode Materials for Lithium Ion Batteries. *ChemSusChem* **2010**, *3*, 236−239.
(10) Lou, X. W.; Deng, D.; Lee, J. Y.; Feng, J.; Archer, L. A. Self-Supported Formation of Needlelike Co_3O_4 Nanotubes and Their Application As Lithium-Ion Battery Electrodes. *Adv. Mater.* **2008**, *20*, 258−262.
(11) Yu, Y.; Chen, C. H.; Shui, J. L.; Xie, S. Nickel-Foam-Supported Reticular CoO-Li_2O Composite Anode Materials for Lithium Ion Batteries. *Angew. Chem., Int. Ed. Engl.* **2005**, *44*, 7085−7089.
(12) Shaju, K. M.; Jiao, F.; Debart, A.; Bruce, P. G. Mesoporous and Nanowire Co_3O_4 As Negative Electrodes for Rechargeable Lithium Batteries. *Phys. Chem. Chem. Phys.* **2007**, *9*, 1837−1842.
(13) Binotto, G.; Larcher, D.; Prakash, A. S.; Herrera Urbina, R.; Hegde, M. S.; Tarascon, J.-M. Synthesis, Characterization, and Li-Electrochemical Performance of Highly Porous Co_3O_4 Powders. *Chem. Mater.* **2007**, *19*, 3032−3040.
(14) (a) Wang, C. B.; Yin, L. W.; Xiang, D.; Qi, Y. X. Uniform Carbon Layer Coated Mn_3O_4 Nanorod Anodes with Improved Reversible Capacity and Cyclic Stability for Lithium Ion Batteries. *ACS Appl. Mater. Interfaces* **2012**, *4*, 1636−1642. (b) Li, Z.; Liu, N.; Wang, X.; Wang, C.; Qi, Y.; Yin, L. Three-Dimensional Nanohybrids of Mn3O4/Ordered Mesoporous Carbons for High Performance Anode Materials for Lithium-Ion Batteries. *J. Mater. Chem.* **2012**, *22*, 16640−16648. (c) Hao, F.; Zhang, Z.; Yin, L. Co_3O_4/Carbon Aerogel Hybrids as Anode Materials for Lithium-Ion Batteries with Enhanced Electrochemical Properties. *ACS Appl. Mater. Interfaces* **2013**, *5*, 8337−8344.
(15) Wang, H. L.; Cui, L. F.; Yang, Y.; Casalongue, H. S.; Robinson, J. T.; Liang, Y. Y.; Cui, Y.; Dai, H. J. Mn_3O_4-Graphene Hybrid as a High-Capacity Anode Material for Lithium Ion Batteries. *J. Am. Chem. Soc.* **2010**, *132*, 13978−13980.
(16) Wu, F.; Chen, J.; Chen, R.; Wu, S.; Li, L.; Chen, S.; Zhao, T. Sulfur/Polythiophene with a Core/Shell Structure: Synthesis and Electrochemical Properties of the Cathode for Rechargeable Lithium Batteries. *J. Phys. Chem. C* **2011**, *115*, 6057−6063.
(17) Wang, J.; Yang, N.; Tang, H.; Dong, Z.; Jin, Q.; Yang, M.; Kisailus, D.; Zhao, H.; Tang, Z.; Wang, D. Accurate Control of Multishelled Co_3O_4 Hollow Microspheres as High-Performance Anode Materials in Lithium-Ion Batteries. *Angew. Chem., Int. Ed. Engl.* **2013**, *52*, 1−5.
(18) Tao, F.; Gao, C.; Wen, Z.; Wang, Q.; Li, J.; Xu, Z. Cobalt Oxide Hollow Microspheres with Micro- and Nano-Scale Composite Structure: Fabrication and Electrochemical Performance. *J. Solid State Chem.* **2009**, *182*, 1055−1060.
(19) Yan, N.; Hu, L.; Li, Y.; Wang, Y.; Zhong, H.; Hu, X.; Kong, X.; Chen, Q. Co_3O_4 Nanocages for High-Performance Anode Material in Lithium-Ion Batteries. *J. Phys. Chem. C* **2012**, *116*, 7227−7235.
(20) Xue, X. Y.; Chen, Z. H.; Xing, L. L.; Yuan, S.; Chen, Y. J. SnO_2/alpha-MoO_3 Core-Shell Nanobelts and Their Extraordinarily High Reversible Capacity As Lithium-Ion Battery Anodes. *Chem. Commun.* **2011**, *47*, 5205−5207.
(21) Cui, L. F.; Yang, Y.; Hsu, C. M.; Cui, Y. Carbon−Silicon Core−Shell Nanowires as High Capacity Electrode for Lithium Ion Batteries. *Nano Lett.* **2009**, *9*, 3370−3374.
(22) Da, D.; Jim, Y. L. Hollow Core−Shell Mesospheres of Crystalline SnO_2 Nanoparticle Aggregates for High Capacity Li^+ Ion Storage. *Chem. Mater.* **2008**, *20*, 1841−1846.
(23) Zhou, L.; Zhao, D.; Lou, X. W. Double-Shelled $CoMn_2O_4$ Hollow Microcubes As High-Capacity Anodes For Lithium-Ion Batteries. *Adv. Mater.* **2012**, *24*, 745−748.
(24) Zhang, L.; Wu, H. B.; Madhavi, S.; Hng, H. H.; Lou, X. W. Formation of Fe_2O_3 Microboxes with Hierarchical Shell Structures From Metal−Organic Frameworks and Their Lithium Storage Properties. *J. Am. Chem. Soc.* **2012**, *134*, 17388−17391.
(25) Xu, X. D.; Cao, R. G.; Jeong, S.; Cho, J. Spindle-Like Mesoporous Alpha-Fe_2O_3 Anode Material Prepared From MOF Template for High-Rate Lithium Batteries. *Nano Lett.* **2012**, *12*, 4988−4991.
(26) Banerjee, A.; Gokhale, R.; Bhatnagar, S.; Jog, J.; Bhardwaj, M.; Lefez, B.; Hannoyer, B.; Ogale, S. MOF Derived Porous Carbon−Fe_3O_4 Nanocomposite As a High Performance, Recyclable Environmental Superadsorbent. *J. Mater. Chem.* **2012**, *22*, 19694−19699.
(27) Wu, R.; Qian, X.; Yu, F.; Liu, H.; Zhou, K.; Wei, J.; Huang, Y. MOF-Templated Formation of Porous CuO Hollow Octahedra for Lithium-Ion Battery Anode Materials. *J. Mater. Chem.A* **2013**, *1*, 11126−11129.
(28) Zhou, H.; Li, D.; Hibino, M.; Honma, I. A Self-Ordered, Crystalline-Glass, Mesoporous Nanocomposite For Use As a Lithium-Based Storage Device with Both High Power and High Energy Densities. *Angew. Chem., Int. Ed. Engl.* **2005**, *44*, 797−802.
(29) Jiang, C.; Hosono, E.; Zhou, H. Nanomaterials for Lithium Ion Batteries. *Nano Today* **2006**, *1*, 28−33.
(30) Bruce, P. G.; Scrosati, B.; Tarascon, J. M. Nanomaterials for Rechargeable Lithium Batteries. *Angew. Chem., Int. Ed. Engl.* **2008**, *47*, 2930−2946.
(31) Li, H.; Shi, L.; Wang, Q.; Chen, L.; Huang, X. Nano-alloy Anode for Lithium Ion Batteries. *Solid State Ionics* **2002**, *148*, 247−258.
(32) Guo, Y.-G.; Hu, J.-S.; Wan, L.-J. Nanostructured Materials for Electrochemical Energy Conversion and Storage Devices. *Adv. Mater.* **2008**, *20*, 2878−2887.
(33) Wu, X.-L.; Jiang, L.-Y.; Cao, F.-F.; Guo, Y.-G.; Wan, L.-J. $LiFePO_4$ Nanoparticles Embedded in a Nanoporous Carbon Matrix: Superior Cathode Material for Electrochemical Energy-Storage Devices. *Adv. Mater.* **2009**, *21*, 2710−2714.
(34) Li, J.; Xiong, S.; Li, X.; Qian, Y. Spinel $Mn_{1.5}Co_{1.5}O_4$ Core−Shell Microspheres as Li-ion Battery Anode Materials with a Long Cycle Life and High Capacity. *J. Mater. Chem.* **2012**, *22*, 23254−23259.
(35) Li, Q.; Yin, L.; Li, Z.; Wang, X.; Qi, Y.; Ma, J. Copper-Doped Hollow Structured Manganese Oxide Mesocrystals with Controlled Phase Structure and Morphology as Anode Materials for Lithium Ion Battery with Improved Electrochemical Performance. *ACS Appl. Mater. Interfaces* **2013**, *5*, 10975−10984.

(36) Jin, S.; Deng, H.; Long, D.; Liu, X.; Zhan, L.; Liang, X.; Qiao, W.; Ling, L. Facile Synthesis of Hierarchically Structured Fe_3O_4/Carbon Micro-flowers and Their Application to Lithium-Ion Battery Anodes. *J. Power Sources* **2011**, *196*, 3887−3893.
(37) Li, W.-Y.; Xu, L.-N.; Chen, J. Co_3O_4 Nanomaterials in Lithium-Ion Batteries and Gas Sensors. *Adv. Funct. Mater.* **2005**, *15*, 851−857.
(38) Liu, J.; Li, Y.; Fan, H.; Zhu, Z.; Jiang, J.; Ding, R.; Hu, Y.; Huang, X. Iron Oxide-Based Nanotube Arrays Derived from Sacrificial Template-Accelerated Hydrolysis: Large-Area Design and Reversible Lithium Storage. *Chem. Mater.* **2010**, *22*, 212−217.
(39) Wu, Z.; Ren, W.; Wen, L.; Gao, L.; Zhao, j.; Chen, Z.; Zhou, G.; Li, F.; Cheng, H. Graphene Anchored with Co_3O4 Nanoparticles as Anode of Lithium Ion Batteries with Enhanced Reversible Capacity and Cyclic Performance. *ACS Nano* **2010**, *4*, 3187−3194.
(40) Yao, W.; Yang, J.; Wang, J.; Nuli, Y. Multilayered Cobalt Oxide Platelets for Negative Electrode Material of a Lithium-Ion Battery. *J. Electrochem. Soc.* **2008**, *155*, A903−A908.
(41) Zhu, J.; Sharma, Y. K.; Zeng, Z.; Zhang, X.; Srinivasan, M.; Mhaisalkar, S.; Zhang, H.; Hng, H. H.; Yan, Q. Cobalt Oxide Nanowall Arrays on Reduced Graphene Oxide Sheets with Controlled Phase, Grain Size, and Porosity for Li-Ion Battery Electrodes. *J. Phys. Chem. C* **2011**, *115*, 8400−8406.
(42) Wang, C.; Chen, J.-j.; Shi, Y.-n.; Zheng, M.-s.; Dong, Q.-f. Preparation and Performance of a Core−Shell Carbon/Sulfur Material For Lithium/Sulfur Battery. *Electrochim. Acta* **2010**, *55*, 7010−7015.
(43) Li, G.-R.; Wang, Z.-L.; Zheng, F.-L.; Ou, Y.-N.; Tong, Y.-X. ZnO@MoO_3 Core/Shell Nanocables: Facile Electrochemical Synthesis and Enhanced Supercapacitor Performances. *J. Mater. Chem.* **2011**, *21*, 4217−4221.
(44) Kim, S.-W.; Ryu, J.; Park, C. B.; Kang, K. Carbon Nanotube-Amorphous $FePO_4$ Core−Shell Nanowires as Cathode Material for Li Ion Batteries. *Chem. Commun.* **2010**, *46*, 7409−7411.